Biomedical Signal Processing and Control 59 (2020) 101890

Contents lists available at ScienceDirect

Biomedical Signal Processing and Control

journal homepage: www.elsevier.com/locate/bspc

Low-density surface electromyographic patterns under electrode shift: Characterization and NMF-based classification

Gan Huang[a,b], Zhien Xian[a,b], Fei Tang[a,b], Linling Li[a,b], Li Zhang[a,b], Zhiguo Zhang[a,b,c,*]

[a] School of Biomedical Engineering, Health Science Center, Shenzhen University, Shenzhen 518060, China
[b] Guangdong Provincial Key Laboratory of Biomedical Measurements and Ultrasound Imaging, Shenzhen University, Shenzhen 518060, China
[c] Peng Cheng Laboratory, Shenzhen, Guangdong, 518055, China

ARTICLE INFO

Article history:
Received 15 April 2019
Received in revised form 15 January 2020
Accepted 11 February 2020

Keywords:
Electrode shift
Surface electromyography
Pattern recognition
Nonnegative matrix Factorization
t-distributed stochastic neighbor embedding

ABSTRACT

Electrode shift causes high variability and non-stationarity in surface electromyographic (sEMG) patterns, which seriously impairs the robustness of sEMG-based prosthetic control in daily use. Existing methods for electrode shift are mostly suitable for high-density sEMG configuration and do not work well for low-density sEMG. Nowadays, a quantitative characterization of the influence of electrode shift on low-density sEMG and an effective classification method to handle the influence of electrode shift are still lacking. The present study first designed an experiment to produce electrode shift in an 8-channel sEMG recording system. By using tSNE and other quantitative indices, we observed that rotating electrodes' position led to great changes in the TD feature space, which subsequently decreased the classification accuracy. Further, we showed that existing algorithms against electrode shift in a high-density electrode configuration have limited effect for low-density sEMG recordings. To combat the influence of electrode shift and to improve the classification accuracy, the nonnegative matrix factorization (NMF) algorithm was used to reduce the non-stationarity of sEMG features and the self-enhancing linear discriminant analysis (SE-LDA) method was adopted to update the classifier based on the changes of sEMG features space. Results showed that the NMF with SE-LDA method achieved an accuracy of 70.58 ± 18.08% for the 10-motion classification problem with electrode shift, which was much higher than the accuracy of 54.84 ± 12.24% achieved by the classical TD features with the LDA classifier. The robust and effective new method against the electrode-shift problem has a great potential for the design of practical sEMG-based prosthetic control.

1. Introduction

Surface electromyography (sEMG) has been extensively used as a control input for upper-limb prosthesis control, which could largely increase the functional capacity of amputees and improve their quality of life [1]. sEMG-based prosthesis control technology provides a natural mapping from upper-limb muscle motions to prosthesis functions with high accuracy and easy operation [2]. For example, by using classical time-domain (TD) features and the linear discriminant analysis (LDA) classifier, an accuracy of > 90% was achieved in the circumstance of 6 motions [3]. However, the high accuracy of sEMG-based motion recognition obtained in laboratory is in sharp contrast to the high rejection rate in practical uses of intelligent prosthetics [4]. Besides the problems of prosthetic weight, battery life, power [5] etc., the low robustness of existing sEMG pattern recognition methods are also an important reason behind the high rejection rate. In daily use, the accuracy of sEMG pattern recognition methods is seriously degraded by several factors, such as electrode shift, changes in arm posture and muscle contraction force, poor electrode contact [6–10]. These factors could remarkably change the sEMG patterns. Consequently, most popular pattern recognition methods, which focus more on the high accuracy in the stationary feature space but less on the robustness to non-stationary environments, cannot achieve good performance under electrode shift.

In recent years, the issue of low robustness of sEMG-based prosthesis control has received increasing attention. Particularly, many methods have been proposed to solve the problem of adverse effects of electrode shift, which is the major source of low robustness of sEMG pattern recognition. For example, Variogram (Variog), a statistical measure of the spatial correlation, could provide

* Corresponding author at: School of Biomedical Engineering, Health Science Center, Shenzhen University, Shenzhen 518060, China.
E-mail address: zgzhang@szu.edu.cn (Z. Zhang).

https://doi.org/10.1016/j.bspc.2020.101890
1746-8094/

robust features for high-density sEMG under electrode shift [11]. Gray-level co-occurrence matrix (GLCM), which provides a well description of spatial distribution of pixels in image processing, can discard information sensitive to shift and keep as much as useful information in electrode shift [12]. Common Spatial Pattern (CSP), which is based on the multiple channels signal analysis, can maximize the difference between the variance of two classes [13]. Electrode shift causes changes in the feature space, so that a classifier trained before electrode shift cannot achieve good performance when being used after electrode shift. Above-mentioned methods have showed improved robustness to electrode shift, but they were developed for high-density sEMG. High-density electrodes have high recognition efficiency and control quality [14], but with the increasing number of the electrodes (> 60 electrodes), the system will need more time to be worn and have a higher risk of breaking single electrode [15]. Furthermore, a high-density sEMG system has much higher requirements for signal acquisition, amplification, transmission and computation, which makes the system more complex and expensive. For these reasons, current high-density sEMG systems are mainly used in laboratory environment, but rarely in daily use.

To date, commercial EMG devices normally use low-density electrodes (for example, Myo armband, Myo, Thalmic Labs, with 8 electrodes) and they are more preferred in daily use for their lower price, easiness-to-wear and acceptable performance. However, it is still unclear whether these high-density electrodes-based methods, like Variog, GLCM and CSP, are still robust against electrode shift for low-density electrodes. Also, to the best of our knowledge, effective methods to cope with the problem of electrode shift in low-density electrode system are still lacking.

The present study is aimed to investigate the electrode shift effects on low-density sEMG signals and to develop a robust pattern recognition method to solve the problem of electrode shift. Firstly, we designed an experiment to produce electrode shift in a 8-channel sEMG configuration. Then we applied t-distributed stochastic neighbor embedding (t-SNE) [16], the quantitative measurement index space distance ratio (SDR), and the confusion matrix, to provide a comprehensive characterization of electrode shift effects on TD features. Last, the nonnegative matrix factorization (NMF) algorithm was used to reduce the non-stationarity of TD features and a self-enhancing linear discriminant analysis (SE-LDA) method was adopted to further improve the classification accuracy.

2. Methods

2.1. Experimental design

Twenty-five able-bodied subjects (18 males and 7 females, aged 22.04 ± 2.07) in this experiment. Ethical approval of the study was sought and obtained from the Medical Ethics Committee, Health Science Center, Shenzhen University (No. 2019004). All subjects were informed of the experimental procedure and signed informed consent before the experiment. Eight-channel sEMG signals were collected from able-bodied subjects' right forearms by SX230 EMG sensor (Biometrics Ltd., Newport, UK) with the sampling rate 1 kHz, input impedance >10,000,000 M Ohms and Common Mode Rejection Ratio typically 110 dB. The stainless-steel bipolar discs electrodes were arranged with a fixed distance of 20 mm with its radius 5 mm [17].

In the preparation stage, the circumference of the arm was measured for each subject. To investigate the circumstance of the electrode shift, the experiment was divided into two parts. In the first part (Fig. 1A), the forearm circumference was divided into 8 equal segments and marked the endpoints clockwise as 1, 2, 3, ..., 8 and the back side of middle finger was set as the origin. In the second part (Fig. 1B), we rotated the electrode positions by 22.5° (roughly 1 cm) clockwise to produce the lateral electrode shift. Since 8 electrodes were evenly arranged on the forearm, the angular difference between adjacent electrodes was 360/8 = 45°. Because there is no any difference among these 8 electrodes and among the features extracted from these 8 electrodes, so a rotation with a degree x (which is greater than 45) is equivalent to a rotation with a degree of y (which is the remainder after division of x by 45). Further, because the rotation could be carried out clockwisely or counterclockwisely, a clockwise rotation with a degree x (which is greater than 22.5 and less than 45) is equivalent to a counterclockwise rotation with a degree of (45-x).

During the whole experiment, the subjects sat in a comfortable chair and kept their arms straight down. Both two parts of the experiment consisted of 10 sessions. For each session, the subjects were asked to complete 10 motions in a random order with 80% mean cumulative voltage for 10 s. These 10 motions (as shown in Fig. 1C) included hand close (HC), hand open (HO), wrist flexion (WF), wrist extension (WE), radial flexion (RF), ulnar flexion (UF), wrist pronation (WP), wrist supination (WS), fine pinch (FP) and rest (RE). The subjects had an adequate rest as he/she wanted between the adjacent two sessions in the experiment. After the completion of the first part of the experiment (Fig. 1A), the position of the electrode was adjusted for the sEMG recording in the second part (Fig. 1B). The sEMG signals recorded from two parts of the experiment were respectively denoted as Dataset 1 and Dataset 2.

2.2. Pre-processing and TD feature extraction

The following preprocessing routines were carried out before feature extraction. The direct current components were removed from sEMG signals. SEMG signals from 2 to 9 s (with a duration of 8 s or 8000 ms) were retained for subsequent analysis and these signals were divided in to 80 non-overlapping epochs, each with a length of 100 ms. Then, four types of TD features [18–20], including Mean Absolute Value (MAV), Waveform Length (WL), Zero Crossings (ZC), and Slope Sign Changes (SSC), were extracted. Hence, we have 8000 samples (80 epochs $\times$ 10 motions $\times$ 10 sessions) and 32 features (4 TD features $\times$ 8 channels) for both Dataset 1 (before electrode shift) and Dataset 2 (after electrode shift).

2.3. Characterizing electrode shift effects

2.3.1. Characterization of feature distribution

Three tools were used to characterize and visualize the effect of electrode shift of sEMG TD features. Firstly, t-distributed stochastic neighbor embedding (t-SNE), as applied as a dimension reduction method for the visualization of the changes in the feature space. Next, a quantitative measurement index space distance ratio (SDR) was used to quantitatively measure the changes. Last, the confusion matrix was adopted to evaluate the influence of the changes in feature space on the classification results for each motion.

2.3.2. t-SNE

Because the dimension of the original feature space was 32, a direct observation of the high dimensional feature space was not possible. Traditional visualization methods, like histograms, scatter plots and parallel coordinate plots [21], could only facilitate the visualization of one or a few features at a time. Here, to visualize the changes of electrode shift of TD features, t-SNE [22] with Mahalanobis distance was applied to embed the high-dimensional feature space into a two-dimension space. As a nonlinear dimension reduction algorithm, t-SNE creates a single map which is capable of capturing local structures of high-dimensional data and revealing global structure well.

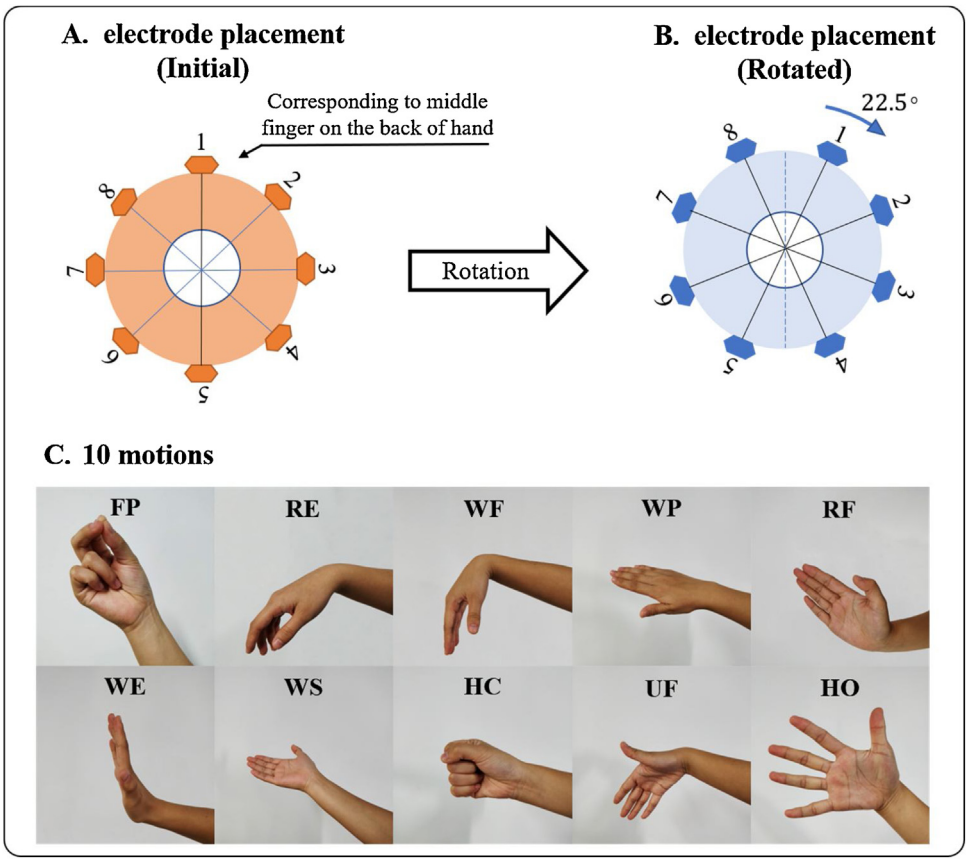

Fig. 1. Experimental design with eight sEMG channels under the electrode shift. A. In the first part of the experiment, the back side of middle finger was set as the origin and the forearm circumference was divided into 8 equal segments. B. In the second part of the experiment, the eight electrodes were rotated 22.5° clockwise to produce the lateral electrode shift. C. sEMG signals of 10 motions were collected in two parts of the experiment.

2.3.3. Space distance ratio

To further quantify the impact of electrode shift on features, the index SDR, which is calculated as the ratio between within-class shift distance (WCSD) and between-class shift distance (BCSD), was used. Suppose there are N_i samples in the subset D_i (samples with class i in Dataset 1), and $\overline{N}_i$ samples in the subset $\overline{D}_i$ (samples with class i in Dataset 2), the corresponding $WCSD_{\overline{x}}$ and $BCSD_{\overline{x}}$ for each sample $\overline{x} \in \overline{D}_i$ in Dataset 2 are

$$WCSD_{\overline{x}} = \frac{1}{N_i}\sum_{x \in D_i} \left\| x - \overline{x} \right\| \tag{1}$$

$$BCSD_{\overline{x}} = \min_{j \neq i} \frac{1}{N_j}\sum_{x \in D_j} \left\| x - \overline{x} \right\| \tag{2}$$

SDR_i for class i is the mean value of the ratio between $WCSD_{\overline{x}}$ and $BCSD_{\overline{x}}$ for all samples $\overline{x} \in \overline{D}_i$ and SDR can be calculated as the mean value of SDR_i of all C classes,

$$SDR_i = \frac{1}{\overline{N}_i}\sum_{\overline{x} \in \overline{D}_i} \left(\frac{WCSD_{\overline{x}}}{BCSD_{\overline{x}}} \right) \tag{3}$$

$$SDR = \frac{1}{C}\sum_{i=1}^{C} SDR_i \tag{4}$$

A small value of SDR (with a small WCSD and a large BCSD) indicates the feature distribution shift has a small impact on the classification result, and vice versa. Here, SDR was proposed as an index to evaluate the property of each method on feature space shift, but not used as a new classifier. Because of the curse of dimensionality, the samples in the high-dimensional space is "far away" from the others which makes the SDR value is always close to 1 in the 32-dimensional raw TD feature space. Hence, SDR value was always calculated in the 2-dimensional space after t-SNE dimension reduction in the analysis. Considering the random factors in the t-SNE method, we repeated the computation of t-SNE 100 times to calculate the mean SDR values.

2.3.4. Confusion matrix

In addition to t-SNE and SDR, we also used the classical confusion matrix to observe the effects of electrode shift on the classification results. The confusion matrix is a special kind of contingency table with two dimensions ("actual" and "predicted"). The diagonal elements represent the classification accuracy of each class, while off-diagonal elements are the mislabeled ratio by the classifier.

2.4. NMF

To combat the adverse influence of electrode shift on classification results, we used NMF to reduce the changes of TD features and used SE-LDA to adaptively update the classifier. NMF [23] was first introduced as follows. Consider the matrix $\boldsymbol{X} \in R^{M \times N}$ with all element nonnegative, in which M is the feature dimension and N denotes the sample size. The NMF can linearly factorize the matrix $\boldsymbol{X}$ into the basis matrix $\boldsymbol{W} \in R^{M \times K}$ and the coefficient matrix $\boldsymbol{H} \in R^{K \times N}$. More precisely, the (m, n)-th element of $\boldsymbol{X}$, X_{mn}, is calculated as

$$X_{mn} \approx (W \cdot H)_{mn} = \sum_{k=1}^{K} W_{mk} H_{kn} \tag{5}$$

Table 1
The NMF algorithm.

Training:	Test:
(1) Initialize $\boldsymbol{W}$ and $\boldsymbol{H}$ as random nonnegative matrices; (2) For $\boldsymbol{iter} = 1, 2, \ldots, \boldsymbol{l}$ $\boldsymbol{W_{mk}} \longleftarrow \boldsymbol{W_{mk}} \left(\sum_{i=1}^{N} \frac{\boldsymbol{X_{mi}}}{\boldsymbol{(WH)_{mi}}} \boldsymbol{H_{ki}} \right)$ $\boldsymbol{W_{mk}} \longleftarrow \frac{\boldsymbol{W_{mk}}}{\boldsymbol{\Sigma_i W_{ik}}}$ $\boldsymbol{H_{kn}} \longleftarrow \boldsymbol{H_{kn}} \left(\sum_{i=1}^{M} \boldsymbol{W_{ik}} \frac{\boldsymbol{X_{in}}}{\boldsymbol{(WH)_{in}}} \right)$ End	(1) Fix W obtained from training and initialize H' as random nonnegative matrices; (2) For $iter = 1, 2, \ldots, l$ $H'_{kn} \longleftarrow H'_{kn} \left(\sum_{i=1}^{M} W_{ik} \frac{X_{in}}{(WH')_{in}} \right)$ End

where K is the intermediate dimension of factorization with $K < NM/(N+M)$. With $M = 32$ and $N = 8000$ ($M << N$), we set $K = 31$ in our application by prior experience. The NMF algorithm can be performed as the following iteration in Table 1. The iteration number l is set to be 400, which is sufficient to guarantee convergence in our test. In this study, we used NMF on TD features under electrode shift and we expected that NMF can reduce the feature changes caused by electrode shift. Hereinafter, TD features after NMF were denoted as NMF features.

2.5. SE-LDA

Self-enhancing LDA [24] (SE-LDA) is an improved version of LDA, and it was use in this study to further improve the classification accuracy. We first briefly introduce the classical LDA. For a two-class classifier problem, suppose that we have a set of N samples, N_1 of which are in the subset D_1 with the label c_1 and N_2 of which are in the subset D_2 with the label c_2. We have the within-class scatter matrix

$$S_w = \sum_{i=1}^{2} S_i \text{ and } S_i = \sum_{x \in D_i} (x - \mu_i)(x - \mu_i)^T \tag{6}$$

where $\mu_i = \frac{1}{N_i} \sum_{x \in D_i} x$, for $i = 1, 2$. If the prior probabilities $P(c_i)$ are the same for c_1 and c_2, the linear discrimination function would be

$$g(x) = [S_w^{-1}(\mu_1 - \mu_2)]^T x - \frac{1}{2}(\mu_1 + \mu_2)^T S_w^{-1}(\mu_1 - \mu_2) \tag{7}$$

If $g(x) > 0$, $x \in c_1$, else $x \in c_2$. For the multiple classification problem, One-versus-One strategy is applied to divide the C-class problem in $C \times (C-1)/2$ binary problems and the classification results come from the majority voting rule.

Above classical LDA method does not consider the non-stationarity of features, which can cause the changes of mean vector μ_i and the scatter matrix S_i. So, the performance of LDA on low-density sEMG classification will be degraded by electrode shift. The SE-LDA method can compensate the slow changes in the features space of sEMG by updating μ_i and S_i to track the non-stationary feature space under electrode shift. Once a test sample x_t is predicted as class i, the mean vector μ_i and the scatter matrix S_i of the class i are updated as

$$\mu_i(t+1) = \frac{n_i \mu_i(t)}{n_i + 1} + \frac{x_t}{n_i + 1} \tag{8}$$

$$S_i(t+1) = S_i(t) + \frac{n_i}{n_i + 1}[x_t - \mu_i(t)][x_t - \mu_i(t)]^T \tag{9}$$

where $\mu_i(t)$ and $S_i(t)$ are functions of sample t, and n_i is the number of samples in class i. By using (8) and (9), the SE-LDA classifier can be recursively updated to accommodate non-stationarity of features.

2.6. Performance evaluation and comparison

To investigate the electrode shift effects on sEMG classification, we firstly took one subject as example to characterize the influence of electrode shift on feature space and classification accuracy, and then performed a group level analysis to evaluate the results of NMF. The classical LDA was first used to prove the increased robustness of NMF features, and then the new SE-LDA method was used on NMF features to further improve the classification accuracy.

For each subject, the EMG signal were collected under two situations (without electrode shift and with electrode shift). The accuracies without electrode shift were calculated from TD and NMF features on Dataset 1 with 10-folder cross validation (CV). The accuracies with electrode shift were obtained from TD and NMF features by training on Dataset 1 and test on Dataset 2. In addition to the TD and NMF features, we also compared other methods to solve the electrode shift problem, including CSP [13], Variog [11] and GLCM [12]. All these methods were originally proposed for high-density sEMG configurations, and they were included here to test their performance in a low-density environment. Without electrode shift, paired-sample t-test was applied to compare the accuracies between TD and NMF. With electrode shift, one-way repeated measures ANOVA was used to tested whether there were significantly difference among TD, NMF, CSP, GLCM, and Variog. After that Bonferroni test was used for post hoc test. All the statistical analyses were performed by using SPSS 23 (IBM corp., NY, USA).

3. Results

3.1. Characterization of TD and NMF Features (Single Subject Analysis)

We first checked the feature distributions without electrode shift (Dataset 1). The distributions of TD and NMF features from Dataset 1 are shown in Fig. 2A and B, respectively. It can be observed that the intra-class variance is increased and the inter-class variance is decreased after NMF decomposition, which is not good for classification. As introduced later in Section 3.3, TD features can achieve higher accuracy than NMF features, if there is no electrode shift.

We can further observe from Fig. 2 that electrode shift caused an offset of the samples with TD features from Dataset 1 (Fig. 2A) to Dataset 2 (Fig. 2C). But the extent and direction of the offset for each class were different, which largely influenced the classification results. Taking UF (purple dots in Fig. 2) and HO (magenta dots in Fig. 2) for example, we can see that, UF is on the left of HO in Fig. 2A, but on the right of class HO in Fig. 2C. For this subject, the SDR for TD feature is 1.72 > 1, which indicated the classification accuracy would be worsen by electrode shift.

With the NMF transformation, an overall offset of the samples in each class from Dataset 1 (Fig. 2B) to Dataset 2 (Fig. 2D) can be observed as well. Compared with the offset for TD features, the offset for NMF features is more consistent for all classes. For example, the relative position between UF and HO is not changed: UF is on the left of classes HO in both Fig. 2B and D. For this subject, the SDR is 1.41 for NMF features, which is smaller than the SDR of 1.72 for TD features. A smaller SDR implies a reduction in the change of the feature space, so the classification accuracy could be improved by using NMF features instead of TD features.

3.2. Comparison of classification accuracy and SDR

The performance among different methods were compared in Fig. 3 for both the original (without Electrode Shift) and the shifted

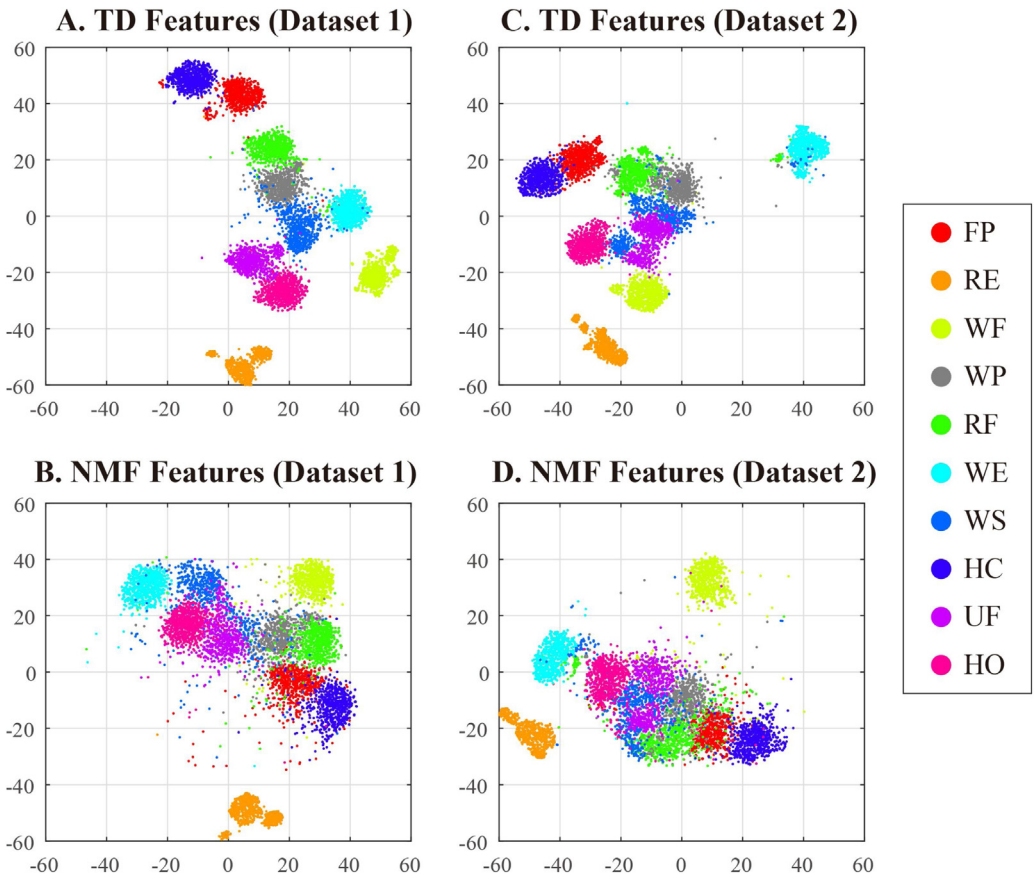

Fig. 2. The distributions of sEMG features (TD features and NMF features, of which the dimension was reduced to 2 by t-SNE) in Dataset 1 (initial electrode placement without electrode shift) and Dataset 2 (rotated electrode placement with electrode shift) of one subject. The x- and y-coordinates indicate the values of t-SNE-reduced features. A. The distribution of TD features in Dataset 1. B. The distribution of NMF features in Dataset 1. C. The distribution of TD features in Dataset 2. D. The distribution of NMF features in Dataset 2.

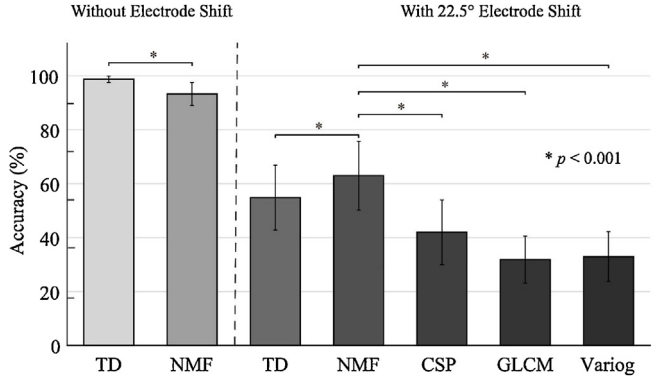

Fig. 3. Comparisons of classification accuracy between different methods with or without electrode shift. The bar graph shows the mean and standard deviation of a method's accuracies across all subjects. The asterisk marker "*" indicates the results from NMF are significantly different from the other methods with $p < 0.001$.

positions (with 22.5 °Electrode Shift). In the original environment (without electrode shift), TD and NMF features were extracted for classification. Paired-sample *t*-test showed the accuracies 95.11 ± 3.43% of NMF method was significantly worse than 98.73 ± 1.16% of TD methods ($p = 5.31 \times 10^{-8}$). For the shifted positions (with 22.5° Electrode Shift), the classification accuracies from TD, NMF, CSP, GLCM, and Variog were compared with LDA classifier. One-way repeated measures ANOVA indicated that there was significantly difference for the mean accuracies among the five methods with $F(4, 96) = 95.736$ and $p < 1.22 \times 10^{-32}$. By using Bonferroni method, the post hoc test results indicated there was significant difference for the mean classification accuracies between each two methods with all the corresponding *p*-value less than 0.001, except the result from the comparison between the methods of GLCM and Variog. The performance of NMF was significantly higher than all the other four methods, which were marked by asterisk in Fig. 3.

The mean SDR for 25 subjects is reduced from 1.40 ± 0.21 for TD features to 1.10 ± 0.20 for NMF features ($p = 5.53 \times 10^{-10}$, paired-sample *t*-test). Hence, the classification accuracies on Dataset 2 under the influence of electrode shift were decreased to 54.84 ± 12.24% for TD features and 64.80 ± 13.92% for NMF features. Some conventional methods, which are robust to the electrode shift in high-density sEMG configuration, had significantly lower accuracies in the low-density sEMG environment (CSP: 42.02 ± 11.99%, Variog: 31.87 ± 8.93%, GLCM: 32.98 ± 9.23%). We can also see that, with the adverse impact of electrode shift, the NMF algorithm could significantly improve the recognition rate because it had significantly higher accuracy than other methods under comparison.

Fig. 4 shows the group-level confusion matrices, in which the values were averaged across all subjects, for TD and NMF features. For TD features, electrode shift had a remarkable negative influence on the recognition of each motion. On the other hand, for NMF features, the accuracies in recognizing almost all motions can be improved to >50%. Some motions, like FP, RE (rest) and WE even had the accuracies more than 80%. Therefore, NMF can significantly

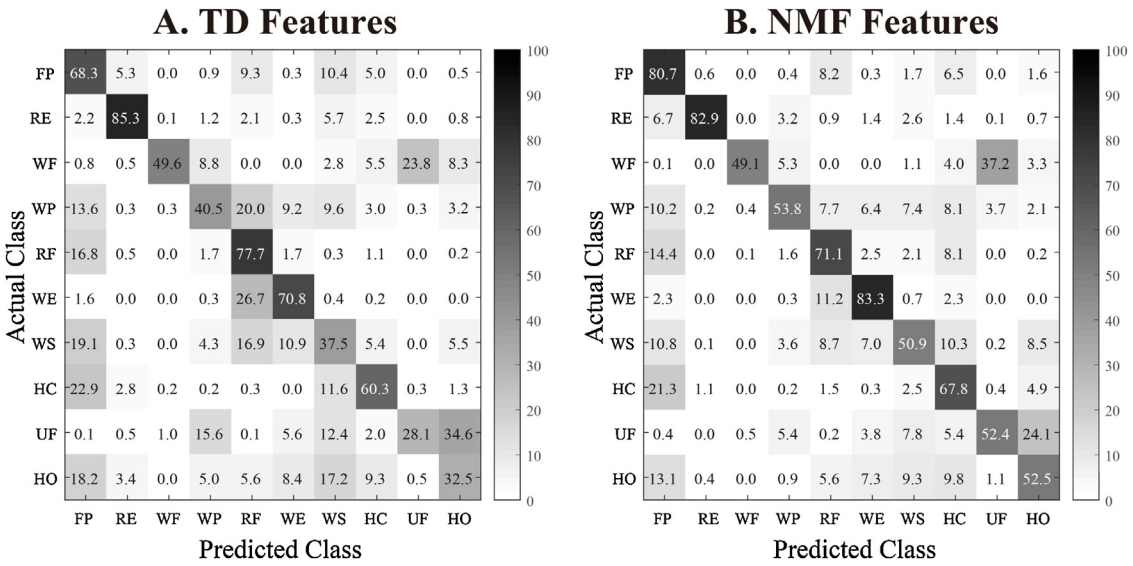

Fig. 4. The confusion matrices obtained by using TD features (A) and NMF features (B) under electrode shift at the group level (averaged across all subjects). The classifiers used to generate the confusion matrices were trained on Dataset 1 and tested on Dataset 2.

increase the classification accuracies and can make the recognition of all motions more stable.

3.3. NMF with SE-LDA

Last, we examined whether SE-LDA can boost the classification accuracy based on NMF features. Fig. 5 shows how the classification accuracies of different methods evolved with the increase of available samples. For each method (each curve), its accuracy can be summarized as the averaged accuracy across all samples. Thus, the classification accuracies of these four methods at the group level are respectively: 54.83 ± 11.99% (TD with LDA), 60.07 ± 15.23% (TD with SE-LDA), 63.92 ± 13.44% (NMF with LDA), and 70.58 ± 18.08% (NMF with SE-LDA). We have the following three main observations: (1) NMF can significantly increase the classification accuracy, as compared with TD features; (2) SE-LDA can further improve the mean accuracies for both TD and NMF features, as compared with LDA; (3) when using SE-LDA, the accuracy of using TD or NMF was gradually improved with the increase of samples and then converged to a steady state, but this phenomenon cannot be observed from LDA-based curves.

4. Discussion

4.1. Changes in distributions of electrode shift

Electrode shift makes great changes in the feature space of low-density sEMG. But the characterization and visualization of TD features under electrode shift are not easy. Because there are 32 TD features from 8 channels, the high-dimensional feature space makes it difficult describe and visualize the electrode shift effects. Therefore, the robustness of a pattern recognition method against electrode shift can only be evaluated by the final classification accuracy, which limits the understanding of the electrode shift problem seriously. In this paper, we used t-SNE to provide an intuitive way to visualize the feature space change caused by electrode shift. By nonlinear dimension reduction, t-SNE maps the high-dimensional data into a low-dimensional space by both capturing most of local structures and revealing global structures well. For TD features, there are small within-class variance and large between-class variance, as shown in Fig. 2. But, when comparing Fig. 2A and C, the electrode shift makes an overall shift, so that the feature space is not stationary. As a result, a TD-based classifier well trained before electrode shift cannot get good performance (98.73 ± 1.16%) when being applied after electrode shift (54.84 ± 12.24%). NMF algorithm can reduce the feature distribution shift efficiently. The trade-off is enlarging the within-class variance. Based on these observations, SDR, which calculates the ratio between within-class shift distance and between-class shift distance, was proposed to evaluate the trade-off (Fig. 2B and D). Here, the value of K in NMF was set to be 31 for a smaller within-class variance.

4.2. Performance evaluation using three indices

In order to evaluate the performance of each method on feature space shift, three quantitative indices are used. First, the overall classification accuracy is the most direct and simplest way to evaluate the effect on each method. The mean accuracy increasing from 54.84 ± 12.24% for TD with LDA to 70.58 ± 18.08% for NMF with SE-LDA, as shown in Fig. 5, is the most direct and powerful evidence to prove the effect of NMF and SE-LDA. Second, the confusion matrix offers a more detailed observation of the classification results. As shown in Fig. 3, the influence of electrode shift was not equal to each class. Some motions, like FP and RE, were recognized well, but some motions, like WP, were misclassified seriously. Compared with TD features, the predict accuracy with NMF features was slightly lower for FP and RE, but much higher for WP. In group-level analysis, it can also be observed that the influence of electrode shift was not equal to each class. NMF features could improve the classification accuracy for classes which performed poor on TD features, such as WP, WS, UF, and HO. Third, SDR was proposed to measure the ratio between within-class shift distance and between-class shift distance. SDR > 1 indicates the classification results would be worsen by electrode shift. SDR was 1.40 ± 0.21 for TD features and 1.10 ± 0.20 for NMF features, which implied electrode shift made the classification of motions more difficult on both TD and NMF features. But the influence of electrode shift on NMF is relatively moderate because its SDR is closer to 1 and smaller than that of TD features. Compared with one simple measure of classification accuracy, the three indices used in this paper provide a more comprehensive assessment of the pattern recognition methods.

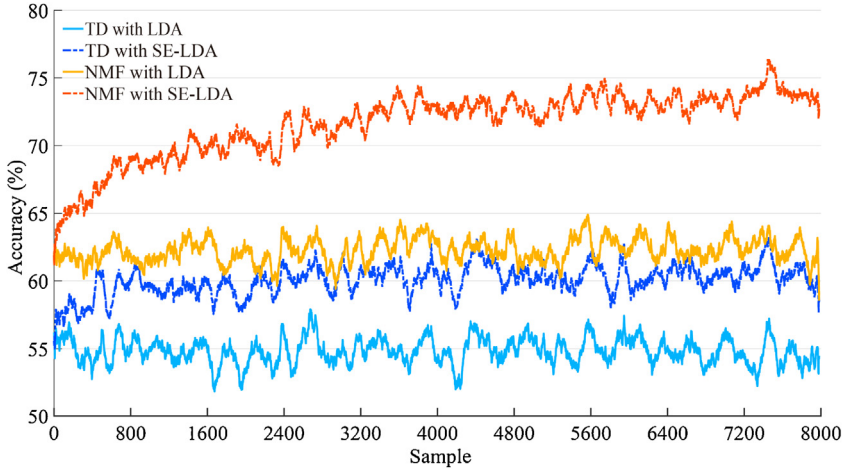

Fig. 5. Classification accuracies evolved with the increase of samples of four methods. The results are averaged from 25 subjects and smoothed using a symmetric window containing 101 adjacent samples.

4.3. NMF and SE-LDA

Existing methods, like CSP, Variog and GLCM, which were proposed to combat the problem of electrode shift with high-density sEMG, cannot work well in the low-density environment. This phenomenon indicates that the low-density sEMG contains limited spatial information, which seriously hinders the performance of CSP, Variog and GLCM. In our study, the NMF algorithm is robust to electrode shift in low-density electrode environment. However, it should be noted that, in the stationary feature space without the influence of electrode shift, NMF cannot improve the accuracy and it actually has a slightly lower accuracy than TD features. To further improve the performance of NMF features, we used an improved version of LDA, SE-LDA, for classification. The new SE-LDA method can recursively and adaptively update important variables (the mean vector and the scatter matrix) used in LDA, so that it can well track the non-stationary environment caused by electrode shift.

4.4. Limitation and future work

The present study was carried out on healthy subjects, but not on amputees. Considering the different degrees of muscle atrophy on amputated patients, the collected sEMG signals would be weaker and with larger variance across subjects. It is even possible that the sEMG signals could not be detected from some muscles. Hence, the problem of electrode shift in sEMG-based prosthetic control for amputees would still be a challenge. It is necessary to examine whether the proposed NMF and SE-LDA method works well on amputees in future work. In addition, the NMF and SE-LDA methods were verified in offline analysis. It is also essential to make a real-time data acquisition and analysis system to realize online implementation of these methods so that they can be used in practice for prosthetic control.

5. Conclusions

In this paper, the problem of electrode shift for prosthetics control with low-density sEMG was studied. The concluding remarks are as follows. First, the non-stationary characteristics of sEMG impair the robustness of prosthetic control in daily use. Existing methods, which were originally proposed to deal with the electrode shift in high-density electrode environment, do not work well for low-density sEMG. Second, the changes of TD feature space caused by electrode shift were visualized by t-SNE and quantified by three types of indices. We found NMF features are better than TD features for motion classification under electrode shift. Third, SE-LDA can further improve the classification accuracy, as compared with LDA. This study can increase our understanding of the electrode shift effects on low-density sEMG and is potentially useful for the design of practical sEMG-based prosthetic limbs.

Acknowledgments

This work was supported by National Natural Science Foundation of China (No. 61701316, No. 81871443), New Entry Teachers' Scientific Research project in Shenzhen University (No. 2018012), Shenzhen Peacock Plan (No. KQTD20160531120514 97) and Science, Technology and Innovation Commission of Shenzhen Municipality Technology Fund (No. JCYJ20170818093322718).

Declaration of Competing Interest

None of the authors have potential conflicts of interest to be disclosed.

References

[1] P. Parker, K. Englehart, B. Hudgins, Myoelectric signal processing for control of powered limb prostheses, J. Electromyogr. Kinesiol. 16 (2006) 541–548.
[2] B. Hudgins, P. Parker, R.N. Scott, A new strategy for multifunction myoelectric control, IEEE Trans. Biomed. Eng. 40 (1993) 82–94.
[3] G. Li, A.E. Schultz, T.A. Kuiken, Quantifying pattern recognition—based myoelectric control of multifunctional transradial prostheses, IEEE Trans. Neural Syst. Rehabil. Eng. 18 (2010) 185–192.
[4] D. Farina, N. Jiang, H. Rehbaum, A. Holobar, B. Graimann, H. Dietl, O.C. Aszmann, The extraction of neural information from the surface EMG for the control of upper-limb prostheses: emerging avenues and challenges, IEEE Trans. Neural Syst. Rehabil. Eng. 22 (2014) 797–809.
[5] M.A. Oskoei, H. Hu, Myoelectric control systems—a survey, Biomed. Signal Process. Control 2 (2007) 275–294.
[6] P. Kaufmann, K. Englehart, M. Platzner, Fluctuating EMG signals: investigating long-term effects of pattern matching algorithms, Annu. Int. Conf. IEEE Eng. Med. Biol., IEEE 2010 (2010) 6357–6360.
[7] A.J. Young, L.J. Hargrove, T.A. Kuiken, The effects of electrode size and orientation on the sensitivity of myoelectric pattern recognition systems to electrode shift, IEEE Trans. Biomed. Eng. 58 (2011) 2537–2544.
[8] D.T. MacIsaac, P.A. Parker, R.N. Scott, K.B. Englehart, C. Duffley, Influences of dynamic factors on myoelectric parameters, IEEE Eng. Med. Biol. Mag. 20 (2001) 82–89.
[9] P.C. Doerschuk, D.E. Gustafon, A.S. Willsky, Upper extremity limb function discrimination using EMG signal analysis, IEEE Trans. Biomed. Eng. (1983) 18–29.
[10] A.J. Young, L.J. Hargrove, T.A. Kuiken, Improving myoelectric pattern recognition robustness to electrode shift by changing interelectrode distance and electrode configuration, IEEE Trans. Biomed. Eng. 59 (2012) 645–652.
[11] A. Stango, F. Negro, D. Farina, Spatial correlation of high density EMG signals provides features robust to electrode number and shift in pattern recognition

for myocontrol, IEEE Trans. Neural Syst. Rehabil. Eng. 23 (2015) 189–198.
[12] J. He, X. Zhu, Combining improved gray-level co-occurrence matrix with high density grid for myoelectric control robustness to electrode shift, IEEE Trans. Neural Syst. Rehabil. Eng. 25 (2017) 1539–1548.
[13] L. Pan, D. Zhang, N. Jiang, X. Sheng, X. Zhu, Improving robustness against electrode shift of high density EMG for myoelectric control through common spatial patterns, J. Neuroeng. Rehabil. 12 (2015) 110.
[14] H. Huang, P. Zhou, G. Li, T.A. Kuiken, An analysis of EMG electrode configuration for targeted muscle reinnervation based neural machine interface, IEEE Trans. Neural Syst. Rehabil. Eng. 16 (2008) 37–45.
[15] P. Zhou, M.M. Lowery, K.B. Englehart, H. Huang, G. Li, L. Hargrove, J.P.A. Dewald, T.A. Kuiken, Decoding a new neural–machine interface for control of artificial limbs, J. Neurophysiol. 98 (2007) 2974–2982.
[16] L. van der Maaten, G. Hinton, Visualizing data using t-SNE, J. Mach. Learn. Res. 9 (2008) 2579–2605.
[17] R. Merletti, P. Di Torino, Standards for reporting EMG data, J. Electromyogr. Kinesiol. 9 (1999) 3–4.
[18] K. Englehart, B. Hudgins, A robust, real-time control scheme for multifunction myoelectric control, IEEE Trans. Biomed. Eng. 50 (2003) 848–854.
[19] H. Huang, F. Zhang, Y.L. Sun, H. He, Design of a robust EMG sensing interface for pattern classification, J. Neural Eng. 7 (2010) 56005.
[20] L.J. Hargrove, K. Englehart, B. Hudgins, A comparison of surface and intramuscular myoelectric signal classification, IEEE Trans. Biomed. Eng. 54 (2007) 847–853.
[21] E. Segel, J. Heer, Narrative visualization: telling stories with data, IEEE Trans. Vis. Comput. Graph. 16 (2010) 1139–1148.
[22] R.A. Jacobs, Increased rates of convergence through learning rate adaptation, Neural Netw. 1 (1988) 295–307.
[23] D.D. Lee, H.S. Seung, Learning the parts of objects by non-negative matrix factorization, Nature 401 (1999) 788.
[24] X. Chen, D. Zhang, X. Zhu, Application of a self-enhancing classification method to electromyography pattern recognition for multifunctional prosthesis control, J. Neuroeng. Rehabil. 10 (2013) 44.